

Deposition of (Ag,Cu)₂Zn(Sn,Ge)S₄ thin films on Mo-coated glass substrate by vacuum magnetron sputtering and post-sulfurization techniques

J. X. Xu^{a,b,*}, X. Tian^a

^a School of Materials and Energy, Guangdong University of Technology, Guangzhou 510006, China

^b School of Integrated Circuits, Guangdong University of Technology, Guangzhou 510006, China

Cation substitution is a useful way to improve the properties of semiconducting Cu₂ZnSnS₄ thin film. In this work, partial Cu and Sn in Cu₂ZnSnS₄ are substituted by Ag and Ge, respectively. The (Ag,Cu)₂Zn(Sn,Ge)S₄ thin films were successfully fabricated using vacuum magnetron sputtering and post-sulfurization techniques. The formation of Ag & Ge co-doped Cu₂ZnSnS₄ structure with secondary phase is proved by XRD and Raman results. The Ag and Ge ratios depend on the composition of Cu-Ag target and the sputtering time of Ge, respectively. The direct optical band gap values of thin films increase with the increase of Ge content. When the sputtering time of Ge is 90 s, the Urbach energy of (Ag,Cu)₂Zn(Sn,Ge)S₄ thin films reaches the minimum value of 339 meV, revealing the reduced band tail state by Ge incorporation.

(Received January 25, 2022; Accepted April 6, 2022)

Keywords: Cu₂ZnSnS₄, Co-doping, Ge substitution, Vacuum sputtering

1. Introduction

In recent years, the quaternary chalcogenides have attracted widespread attentions for application in optoelectronic devices. The typical quaternary chalcogenide is semiconducting Cu₂ZnSnS₄ thin film which has high absorption coefficient of 10⁴ cm⁻¹ order of magnitude [1-3]. Only a thickness of 1~2 μm is needed for Cu₂ZnSnS₄ as an absorber of thin film solar cell. Cu₂ZnSnS₄ has a direct band gap of about 1.5 eV, which meets the requirement for an absorber in a single-junction solar cell [1-3]. In addition, the high abundance and low production cost of Cu, Zn, Sn, and S elements make Cu₂ZnSnS₄ becomes a potential candidate of CuInSe₂ and CdTe solar energy materials which contain scarce or toxic elements [4,5].

Nowadays, the developing of Cu₂ZnSnS₄ thin film solar cells is fast and the conversion efficiency of solar cells has been improved to about 12.7% [6]. Further enhancement in Cu₂ZnSnS₄ thin film solar cells is mainly limited by the open-circuit voltage loss which is related to the defect states in Cu₂ZnSnS₄ absorber [7,8]. There are many point defects and defect clusters in Cu₂ZnSnS₄ thin film [5, 9-12]. The Cu and Zn sites in Cu₂ZnSnS₄ lattice are equivalence, so Zn atoms are easily to be replaced by Cu atoms, leading to the formation of Cu-Zn disorder, Cu_{Zn} anti-site defect,

*Corresponding author xujiaxiong@gdut.edu.cn

<https://doi.org/10.15251/JOR.2022.182.227>

and V_{Cu} vacancy defect. The Cu_{Zn} and V_{Cu} defects can lead to the recombination of photo-generated carriers [13-15]. In addition, Sn has +4 and +2 states, which favor the formation of related defects. The Sn_{Zn} is deep-level defect which is harmful to the photovoltaic performances of Cu_2ZnSnS_4 solar cell [16]. The $[Cu_{Zn}+Sn_{Zn}]$ defect cluster can also be found in Cu_2ZnSnS_4 [17]. Most defects in Cu_2ZnSnS_4 lead to the loss of photo-generated carriers and reduction in the open-circuit voltage and conversion efficiency of solar cells. Therefore, it urgently needs to explore effective way to reduce the defects in Cu_2ZnSnS_4 thin film.

In addition to optimize the preparation process, it has been reported that partial or full substitution of cation in Cu_2ZnSnS_4 by external ions can improve the properties of Cu_2ZnSnS_4 thin films and solar cells [18-22]. The substitution of Cu^+ by Ag^+ can reduce the Cu_{Zn} anti-site defects and V_{Cu} vacancy defects, enlarge the grain size of Cu_2ZnSnS_4 , and increase the conversion efficiency of Cu_2ZnSnS_4 solar cells [18,19]. The Cu_{Zn} defects can also be reduced by the substitution of Zn^{2+} by Cd^{2+} , Fe^{2+} , Mn^{2+} , Mg^{2+} , or Co^{2+} [20-22]. The Sn atoms in Cu_2ZnSnS_4 thin film can be replaced by Si or Ge atoms to reduce the formation of Sn_{Zn} defects and the loss of volatile Sn or Sn-S during sulfurization reaction. Most reports involve single substitution that uses one external dopant to partially or fully replace one element in Cu_2ZnSnS_4 lattice. Recently, double substitution (also called co-doping) of Cu_2ZnSnS_4 has been proposed [23-27]. Two kinds of cation in Cu_2ZnSnS_4 are partially substituted by corresponding equivalent ions. The co-doping combinations of Ag & Cd [23], Ag & Mn [24,25], Ag & Ge [26], Li & Ag [27,28], and Li & Cd [27] have been proposed to provide better effects on reduced defects in Cu_2ZnSnS_4 and enhanced photovoltaic performance of Cu_2ZnSnS_4 solar cells. J.J. Fu et al. used solution method to prepare Ag & Ge co-doped Cu_2ZnSnS_4 with doping gradient. The Ag & Ge co-doping has synergistic effect on regulation of band diagram and reduction in defect of Cu_2ZnSnS_4 . In our previous published works, the influences of the concentrations of Ag and Mn on co-doped Cu_2ZnSnS_4 thin film were studied [24,25]. The Ag & Mn co-doped Cu_2ZnSnS_4 shows better properties than Ag single-doped and Mn single-doped Cu_2ZnSnS_4 .

As the Cu_{Zn} and Sn_{Zn} are dominate defects in Cu_2ZnSnS_4 and play key role in the performance of solar cell, the double substitution of Cu and Sn sites in Cu_2ZnSnS_4 seems to be more attractive. The reported work used chemical solution method to fabricate Ag & Ge co-doped Cu_2ZnSnS_4 [26]. On the other hand, vacuum sputtering technique shows advantage of reduced contamination during thin film preparation, and improved crystallinity and uniformity of thin film, etc. It can use elemental Ge target to sputter Ge-doped Cu_2ZnSnS_4 thin film. To the best of our knowledge, fabrication of co-doped Cu_2ZnSnS_4 thin film by vacuum sputtering method has not been published.

In present work, Ag & Ge co-doped Cu_2ZnSnS_4 thin films were deposited by sputtering and sulfurization. A Cu-Ag alloy target was utilized for Ag doping, and a Ge layer was introduced into the stacked precursor to realize Ge doping. The Ge ratio of co-doped thin films was adjusted by Ge sputtering time. The structures, compositions, morphologies, and optical properties of Ag & Ge co-doped Cu_2ZnSnS_4 thin films were investigated.

2. Experimental

Figure 1 shows schematic diagram of the fabrication of $(Ag,Cu)_2Zn(Sn,Ge)S_4$ thin film.

Soda-lime glasses with size of 2.5 cm × 2.5 cm × 1 mm were used as substrate of (Ag,Cu)₂Zn(Sn,Ge)S₄ thin films and soaked sequentially in acetone, ethanol, and deionized water in a ultrasonic cleaning machine (JP-040S) to remove contaminants on the surface. Each step of ultrasonic cleaning was performed for 15 min. After dried by nitrogen flow, the substrates were transferred into a FJL560 magnetron sputtering instrument produced by Sky Technology Development Co., LTD. The vacuum chamber was evacuated to a base pressure of 5 × 10⁻⁴ Pa. Then, high-purity Ar was introduced into the chamber with a flow of 20 ml/min. Mo back electrode was deposited on the surface of glass substrates by a two-step direct current sputtering. In the first step, the working pressure and sputtering time were 2 Pa and 5 min, respectively, to ensure a good adhesion between Mo and glass. The second step used a low working pressure of 0.5 Pa and sputtering time of 33 min to reduce the resistivity of Mo. Both sputtering powers for the two steps were 50 W. The total thickness of Mo was about 1 μm. (Ag,Cu)₂Zn(Sn,Ge)S₄ precursors were sputtered using a stacked structure of Zn/Sn/Ge/Cu-Ag as shown in Figure 1. The elemental Zn, Sn, and Ge targets and Cu-Ag alloy target with atomic ratio of Cu:Ag=9:1 were used for the sputtering of precursor. Table 1 lists the sputtering conditions of each target. Four samples were prepared with different sputtering times of Sn and Ge to study the effect of Ge ratio on thin film. During the sputtering of precursors, the argon flow and working pressure were kept at 20 ml/min and 0.5 Pa, respectively.

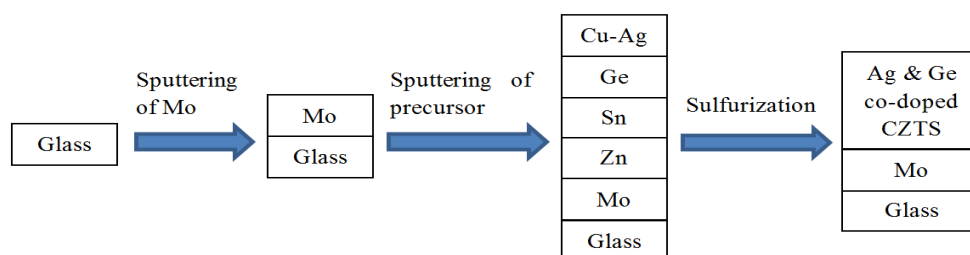


Fig. 1. Schematic diagram of the preparation of (Ag,Cu)₂Zn(Sn,Ge)S₄ thin film.

Table 1. The sputtering times (s) of each target for (Ag,Cu)₂Zn(Sn,Ge)S₄ precursor.

Sample	Zn	Sn	Ge	Cu-Ag
#1	92	170	30	420
#2	92	140	60	420
#3	92	110	90	420
#4	92	80	120	420

The prepared precursors were further sulfurized in a tube furnace to obtain the final (Ag,Cu)₂Zn(Sn,Ge)S₄ thin films. Solid sulfur powders with a mass of 2 g were utilized as sulfur source. The furnace temperature was risen from room temperature to 550 °C and then kept for 1 hour. During heat treatment, the sulfur powders were evaporated and the precursors were sulfurized under the sulfur atmosphere. High-purity nitrogen was introduced into the quartz tube as protective gas during the whole sulfurization process.

X-ray diffractometer (XRD, Rigaku D/MAX-Ultima IV) was used for the analysis of the crystal structure of fabricated samples. The phase of thin films was further identified by Raman spectrometer (Finder Vista) using incident laser with a wavelength of 532 nm. The compositional properties of thin films were measured by X-ray energy dispersive spectroscopy (EDS, IXRF Systems, SDD3030). The morphologies of samples were observed using field emission scanning electron microscope (Hitachi SU8010). The reflectivity and transmittance of thin films were measured by ultraviolet-visible spectrophotometer (UV-3600 Plus). Since Mo was opaque, $(\text{Ag,Cu})_2\text{Zn}(\text{Sn,Ge})\text{S}_4$ thin films directly deposited on glass substrate without Mo were also prepared for the measurements of optical properties.

3. Results and discussion

Figure 2 provides the XRD patterns of $(\text{Ag,Cu})_2\text{Zn}(\text{Sn,Ge})\text{S}_4$ thin films with different sputtering times of Ge. According to the standard XRD data, the XRD peaks of the preferred (112) plane of $\text{Cu}_2\text{ZnSnS}_4$ (PDF#26-0575), $\text{Ag}_2\text{ZnSnS}_4$ (PDF#35-0544), and $\text{Cu}_2\text{ZnGeS}_4$ (PDF#25-0327) locate at 28.53° , 27.28° , and 29.06° , respectively. In Figure 2, the peaks near 28° for all samples are attributed to the (112) plane. The peak positions of samples with Ge sputtering times of 30 s and 60 s match with the $\text{Cu}_2\text{ZnSnS}_4$ phase. The (112) peaks of samples with Ge sputtering times of 90 s and 120 s shift to right and locate between the peaks of $\text{Cu}_2\text{ZnSnS}_4$ and $\text{Cu}_2\text{ZnGeS}_4$, indicating the incorporation of Ge into thin film. The peak position shifts to right with increasing Ge sputtering time because Ge has smaller ion radius than Sn. In addition to the (112) peak, the peaks near 47.5° and 56.4° come from the (220) and (312) planes of co-doped $\text{Cu}_2\text{ZnSnS}_4$, respectively. The changes of (220) and (312) peaks with Ge sputtering time are similar with those of (112) peak. The reported Ge single-doped $\text{Cu}_2\text{ZnSnS}_4$ also shows shift of XRD peaks [29,30]. The peaks near 21.5° reveal that all samples contain secondary phase of Sn_2S_3 , which may result from the incomplete sulfurization reaction or the non-stoichiometry of prepared samples. The Mo peaks at 40.7° originate from the Mo back electrodes.

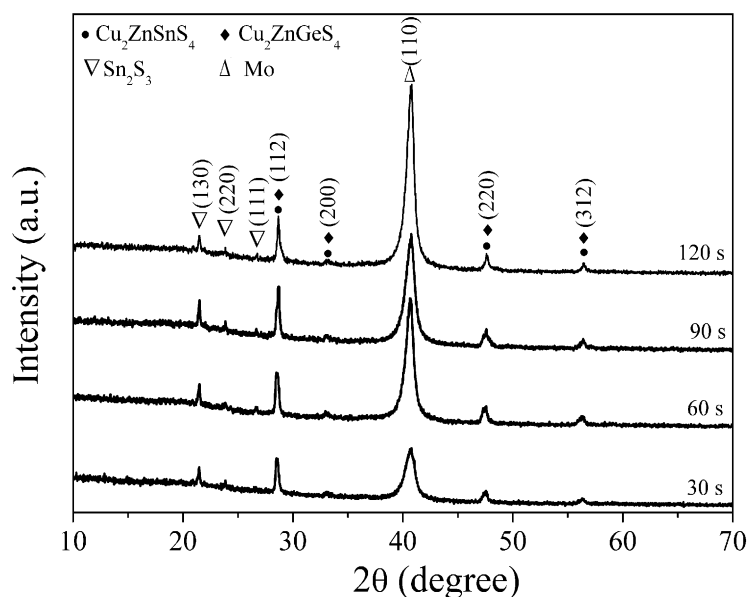


Fig. 2. XRD patterns of $(\text{Ag,Cu})_2\text{Zn}(\text{Sn,Ge})\text{S}_4$ thin films with different sputtering times of Ge.

Figure 3 presents the Raman spectra of $(\text{Ag,Cu})_2\text{Zn}(\text{Sn,Ge})\text{S}_4$ thin films with different sputtering times of Ge. All Raman spectra show characteristic peak at wavenumber of around 330 cm^{-1} . According to Ref. [31], this Raman characteristic peak is ascribed to the A_1 vibration mode of $\text{Cu}_2\text{ZnSnS}_4$, indicating the formation of $\text{Cu}_2\text{ZnSnS}_4$ phase after sulfurization. The Raman peaks at 330 cm^{-1} have no significant change with the sputtering time of Ge. These results reveal that the incorporation of Ag and Ge into $\text{Cu}_2\text{ZnSnS}_4$ has slight influence on the vibration mode of $\text{Cu}_2\text{ZnSnS}_4$. In Figure 3, except the peak at 330 cm^{-1} , other related Raman peaks can not be effectively detected. The XRD and Raman results suggest the formation of Ag & Ge co-doped $\text{Cu}_2\text{ZnSnS}_4$ structure with secondary phases.

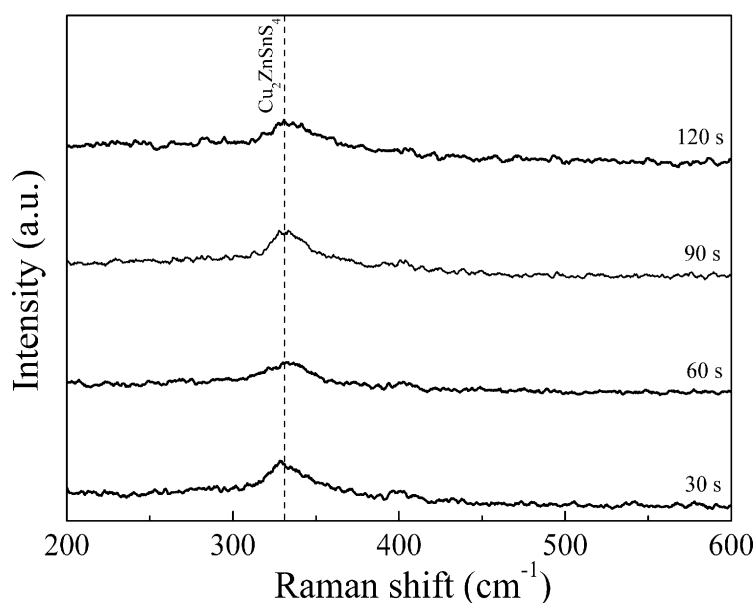


Fig. 3 Raman spectra of $(\text{Ag,Cu})_2\text{Zn}(\text{Sn,Ge})\text{S}_4$ thin films with different sputtering times of Ge.

Figure 4 shows the EDS spectra of $(\text{Ag,Cu})_2\text{Zn}(\text{Sn,Ge})\text{S}_4$ thin films with different sputtering times and Table 2 lists the atomic percentages of Cu, Zn, Sn, S, Ag, and Ge, and the atomic ratios of $\text{Ag}/(\text{Ag}+\text{Cu})$, $\text{Ge}/(\text{Ge}+\text{Sn})$, $(\text{Ag}+\text{Cu})/(\text{Zn}+\text{Ge}+\text{Sn})$, $\text{Zn}/(\text{Ge}+\text{Sn})$, and $\text{S}/(\text{Cu}+\text{Zn}+\text{Sn}+\text{Ag}+\text{Ge})$ for each sample. The values of $\text{Ag}/(\text{Ag}+\text{Cu})$ of all samples are close to the atomic ratio of the Cu-Ag alloy target. The atomic percentage of Ge and the atomic ratio of $\text{Ge}/(\text{Ge}+\text{Sn})$ increase monotonously with the increase of sputtering time of Ge. Therefore, the Ge content can be adjusted by the sputtering time of Ge during the preparation of precursor. The $(\text{Ag}+\text{Cu})/(\text{Zn}+\text{Ge}+\text{Sn})$ values of all samples are lower than 1. The values of $\text{Zn}/(\text{Ge}+\text{Sn})$ of all samples are larger than 1. The Zn-rich composition of prepared thin films is beneficial to the absorber application in solar cell [32,33]. The ratio of $\text{S}/(\text{Cu}+\text{Zn}+\text{Sn}+\text{Ag}+\text{Ge})$ is close to the stoichiometry of 1, indicating the effective sulfurization of precursor.

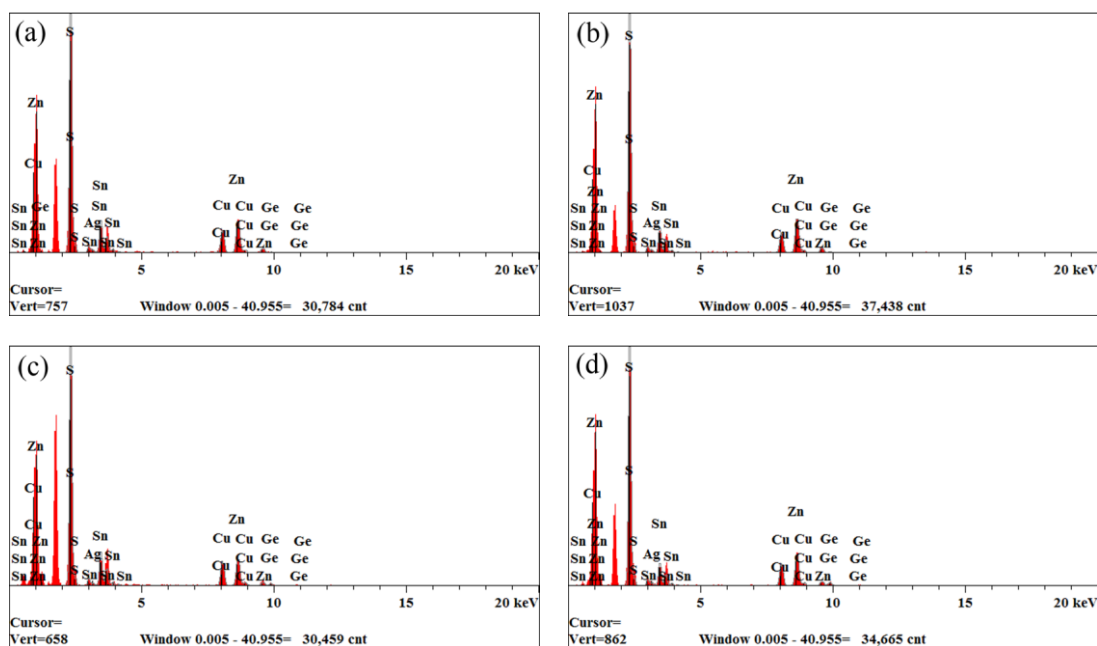


Fig. 4 EDS spectra of $(\text{Ag,Cu})_2\text{Zn}(\text{Sn,Ge})\text{S}_4$ thin films with the Ge sputtering time of (a) 30 s, (b) 60 s, (c) 90 s, and (d) 120 s.

Table 2. Composition of $(\text{Ag,Cu})_2\text{Zn}(\text{Sn,Ge})\text{S}_4$ thin films with different sputtering times of Ge.

Composition	Sputtering time of Ge (s)			
	30	60	90	120
Cu (at. %)	13.41	12.32	15.03	13.31
Zn (at. %)	23.45	26.14	20.01	22.68
Sn (at. %)	9.18	7.29	9.72	6.45
S (at. %)	51.35	50.72	50.60	51.31
Ag (at. %)	1.67	1.79	1.94	2.03
Ge (at. %)	0.94	1.73	2.71	4.23
Ag/(Ag+Cu)	0.11	0.13	0.11	0.13
Ge/(Ge+Sn)	0.09	0.19	0.22	0.40
(Ag+Cu)/(Zn+Ge+Sn)	0.45	0.40	0.52	0.46
Zn/(Ge+Sn)	2.32	2.90	1.61	2.12
S/(Cu+Zn+Sn+Ag+Ge)	1.06	1.03	1.02	1.05

Figure 5 shows the surface SEM images of $(\text{Ag,Cu})_2\text{Zn}(\text{Sn,Ge})\text{S}_4$ thin films with different Ge contents. In Figure 5(a), when the Ge sputtering time is 30 s, the surface of sample consists of grains with the maximum size of about 300 nm. Some voids appear on the thin film surface possibly due to the evaporation of volatile sulfide during sulfurization treatment. When the Ge sputtering time increases to 60 s, the thin film surface becomes irregularity and the grain size is slightly smaller than that in Figure 5(a). For the thin film with Ge sputtering time of 90 s, in Figure 5(c), the thin film surface is compact and the grain aggregation becomes more significant. Finally,

in Figure 5(d), when the Ge sputtering time further increases to 120 s, the grains of $(\text{Ag,Cu})_2\text{Zn}(\text{Sn,Ge})\text{S}_4$ thin films enlarge with the maximum size of about 500 nm.

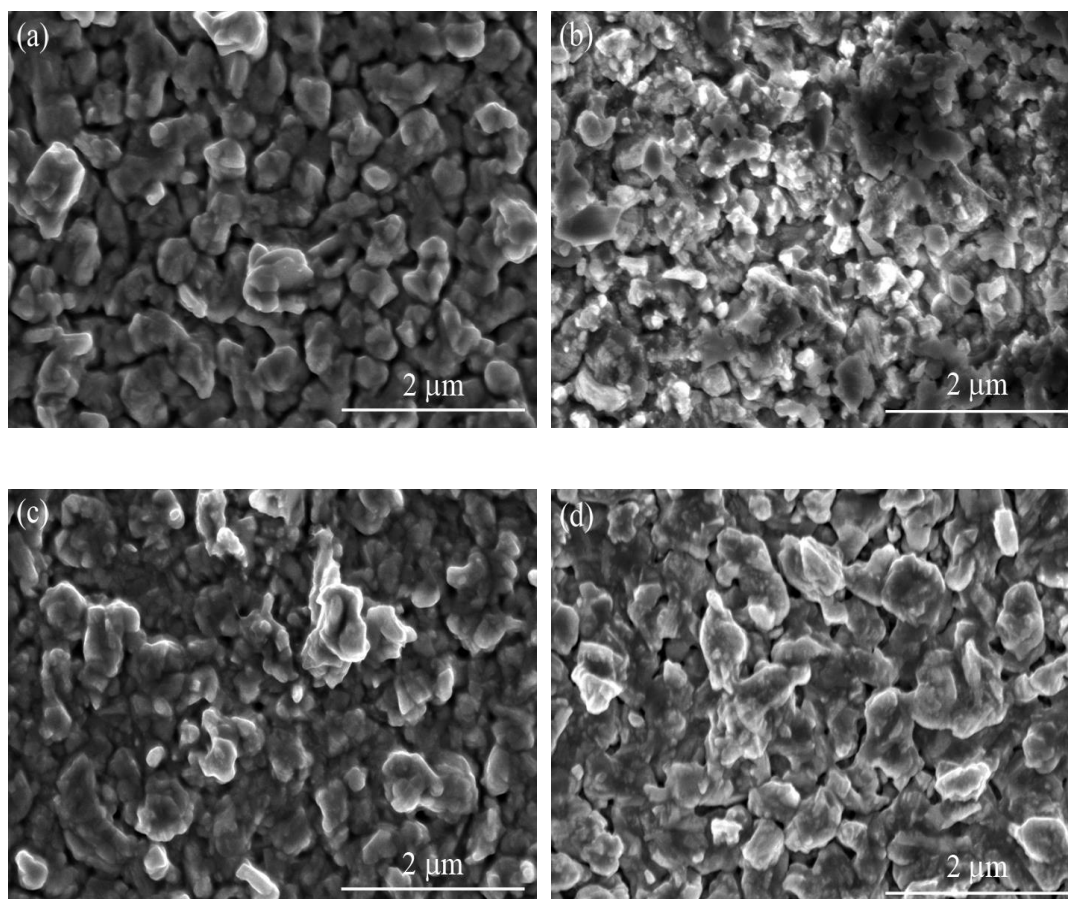


Fig. 5. SEM images of $(\text{Ag,Cu})_2\text{Zn}(\text{Sn,Ge})\text{S}_4$ thin films with the Ge sputtering time of (a) 30 s, (b) 60 s, (c) 90 s, and (d) 120 s.

The reflectivity and transmittance of $(\text{Ag,Cu})_2\text{Zn}(\text{Sn,Ge})\text{S}_4$ thin films in the wavelength range from 400 nm to 1000 nm are provided in Figure 6. In Figure 6(a), the average reflectivity of $(\text{Ag,Cu})_2\text{Zn}(\text{Sn,Ge})\text{S}_4$ thin films in the visible region from 400 nm to 780 nm is 8.8%, 11.1%, 11.2%, and 8.7% when the Ge sputtering times are 30 s, 60 s, 90 s, and 120 s, respectively. The reflectivity of Ag & Ge co-doped $\text{Cu}_2\text{ZnSnS}_4$ thin film is lower than that of Ag & Mn co-doped $\text{Cu}_2\text{ZnSnS}_4$ thin film in Ref. [24], which may result from the rough surfaces of $(\text{Ag,Cu})_2\text{Zn}(\text{Sn,Ge})\text{S}_4$ thin films. A low reflectivity of thin film is beneficial to enhance absorption coefficient of thin film. In Figure 6(b), the transmittance of all thin films reduces with the decrease of wavelength due to the absorption of incident photons. The transmittance of $(\text{Ag,Cu})_2\text{Zn}(\text{Sn,Ge})\text{S}_4$ thin films reduce to near zero when the wavelength is lower than 500 nm.

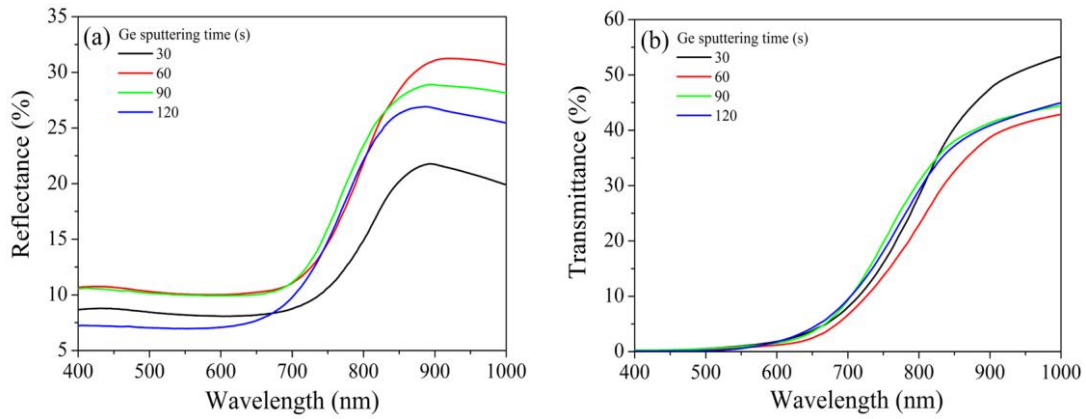


Fig. 6 The (a) reflectivity and (b) transmittance of $(\text{Ag,Cu})_2\text{Zn}(\text{Sn,Ge})\text{S}_4$ thin films with different sputtering times of Ge.

Based on the measured reflectivity and transmittance in Figure 6, the absorption coefficients (α) of $(\text{Ag,Cu})_2\text{Zn}(\text{Sn,Ge})\text{S}_4$ thin films are calculated using the equation [2]

$$\alpha = -\frac{1}{d} \ln \left\{ \frac{T^2 - (1-R)^2 + \sqrt{4T^2 + [(1-R)^2 - T^2]^2}}{2T} \right\} \quad (1)$$

where d , T , and R are the thickness, transmittance, and reflectivity of thin film, respectively. Figure 7 shows the change of absorption coefficients of $(\text{Ag,Cu})_2\text{Zn}(\text{Sn,Ge})\text{S}_4$ thin films with photon energy ($h\nu$). The average absorption coefficients of $(\text{Ag,Cu})_2\text{Zn}(\text{Sn,Ge})\text{S}_4$ thin films in the photon energy range from 1.59 eV to 2.6 eV are $3.4 \times 10^4 \text{ cm}^{-1}$, $3.7 \times 10^4 \text{ cm}^{-1}$, $3.4 \times 10^4 \text{ cm}^{-1}$, and $3.6 \times 10^4 \text{ cm}^{-1}$ for samples with the Ge sputtering times of 30 s, 60 s, 90 s, and 120 s, respectively, which are comparable in the same magnitude of absorption coefficients of $\text{Cu}_2\text{ZnSnS}_4$ thin films with and without substitution in our previous works [2,24,25]. These results indicate promising absorption property of Ag & Ge co-doped $\text{Cu}_2\text{ZnSnS}_4$ thin film.

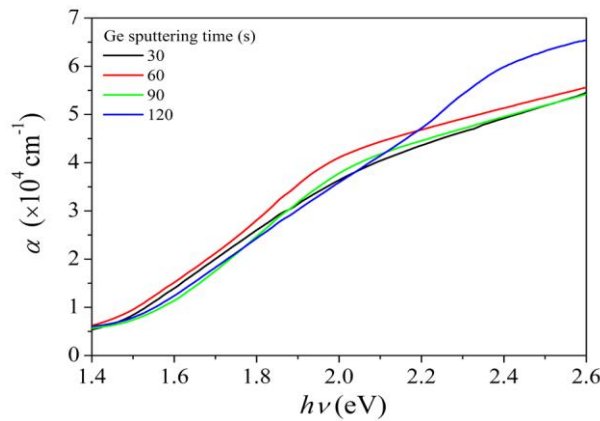


Fig. 7. The absorption coefficients of $(\text{Ag,Cu})_2\text{Zn}(\text{Sn,Ge})\text{S}_4$ thin films with different sputtering times of Ge.

The band gap of thin film can be deduced from the absorption coefficient using the relation $(\alpha h\nu)^n = C(h\nu - E_g)$, where the exponent $n=2$ and $n=1/2$ relate to direct and indirect optical band gaps, respectively, C is a constant, and E_g is the optical band gap of thin film. Figure 8 shows the $(\alpha h\nu)^2$ versus $h\nu$ curves of $(\text{Ag,Cu})_2\text{Zn}(\text{Sn,Ge})\text{S}_4$ thin films with different sputtering times of Ge. The linear region of each curve is found and the epitaxial lines are drawn to get the intercept on the $h\nu$ axis, which is the direct optical band gap. The optical band gaps of samples with the Ge sputtering times of 30 s, 60 s, 90 s, and 120 s are 1.81 eV, 1.84 eV, 1.92 eV, and 2.0 eV, respectively. The direct optical band gap of $(\text{Ag,Cu})_2\text{Zn}(\text{Sn,Ge})\text{S}_4$ thin films increases with the increase of Ge content, which is in agreement with the published results for Ge single substituted $\text{Cu}_2\text{ZnSnS}_4$ thin films [34-36]. The increase of direct optical band gap of $(\text{Ag,Cu})_2\text{Zn}(\text{Sn,Ge})\text{S}_4$ is considered to be due to the upward shift of the bottom of the conduction band induced by higher energy level of Ge than Sn.

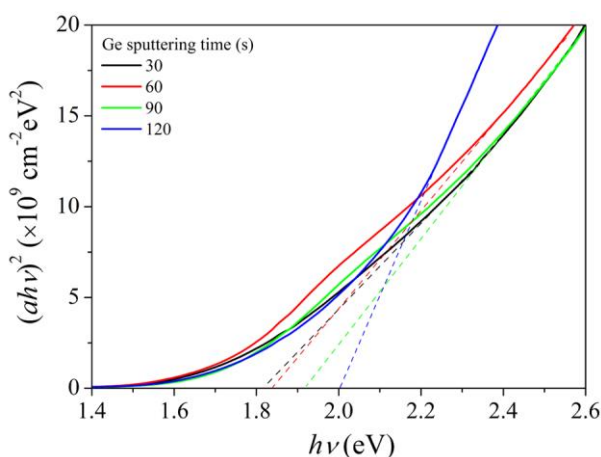


Fig. 8. The $(\alpha h\nu)^2$ versus $h\nu$ curves of $(\text{Ag,Cu})_2\text{Zn}(\text{Sn,Ge})\text{S}_4$ thin films with different sputtering times of Ge.

The band tail state of thin film can be identified by Urbach energy (E_u). The relationship between Urbach energy and absorption coefficient is given by

$$\alpha = \alpha_0 \exp\left(\frac{h\nu}{E_u}\right) \quad (2)$$

where α_0 is a constant. Hence, the Urbach energy can be obtained from the $\ln(\alpha)$ versus $h\nu$ curve. Using the absorption coefficients of $(\text{Ag,Cu})_2\text{Zn}(\text{Sn,Ge})\text{S}_4$ thin films in Figure 7, the $\ln(\alpha)$ - $h\nu$ curves are calculated and plotted in Figure 9. Epitaxial lines of the linear region of the $\ln(\alpha)$ - $h\nu$ curves are also shown in Figure 9. According to Eq. (2), the reciprocal of the slope of epitaxial line is the Urbach energy. The calculated results show that the Urbach energies of $(\text{Ag,Cu})_2\text{Zn}(\text{Sn,Ge})\text{S}_4$ thin films with Ge sputtering times of 30 s, 60 s, 90 s, and 120 s are 380 meV, 357 meV, 339 meV, and 396 meV, respectively. A suitable increase of Ge content can reduce the Sn related defects, resulting in the decrease of Urbach energy and band tail state of

(Ag,Cu)₂Zn(Sn,Ge)S₄ thin films. This is beneficial to reduce the recombination of carriers and enhance the photovoltaic properties of solar cells. However, an excess Ge ratio induces additional defects and leads to the increase of Urbach energy.

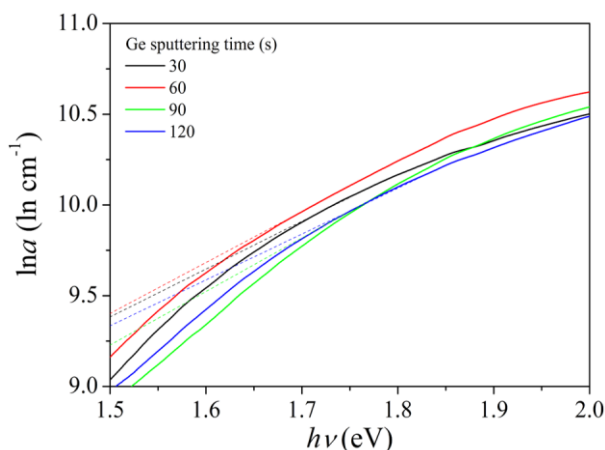


Fig. 9. The relationship between $\ln \alpha$ and $h\nu$ of $(\text{Ag,Cu})_2\text{Zn}(\text{Sn,Ge})\text{S}_4$ thin films with different sputtering times of Ge.

4. Conclusion

Ag & Ge co-doped Cu₂ZnSnS₄ thin films were fabricated by vacuum sputtering and post-sulfurization. A Zn/Sn/Ge/Cu-Ag stacked precursor was designed to realize the Ag & Ge co-doping. The XRD and Raman results indicate the successful formation of polycrystalline (Ag,Cu)₂Zn(Sn,Ge)S₄ with preferred orientation along the (112) plane. The ratio of Ge influences the positions of XRD peaks. The atomic ratio of Ag/(Ag+Cu) of thin film is close to that of Cu-Ag alloy target. The Ge content can be adjusted by the sputtering time of Ge. The atomic percentage of S of prepared samples is near 50%, indicating the effective sulfurization of precursor. With the increase of the sputtering time of Ge, the grains distributed on the thin film surface have larger size. The average reflectivity of (Ag,Cu)₂Zn(Sn,Ge)S₄ thin films in the visible region gets the lowest when the sputtering time of Ge is 120 s. The prepared (Ag,Cu)₂Zn(Sn,Ge)S₄ thin films show promising absorption property with absorption coefficients in the order of magnitude of 10⁴ cm⁻¹. The direct optical band gaps of (Ag,Cu)₂Zn(Sn,Ge)S₄ thin films increase with the increase of Ge content. The band tail state of (Ag,Cu)₂Zn(Sn,Ge)S₄ can be inhibited by a suitable Ge content.

References

- [1] Nisika, K. Kaur, M. Kumar, J. Mater. Chem. A 8, 21547 (2020); <https://doi.org/10.1039/D0TA06450E>
- [2] L. Qiu, J.X. Xu, W.T. Cai, Z.W. Xie, Y.Z. Yang, Superlattices Microstruct. 126, 83 (2019); <https://doi.org/10.1016/j.spmi.2018.12.020>
- [3] X.M. Huang, J.H. Lin, J.X. Xu, Y.Q. Liu, Y.Z. Yang, Z.W. Xie, W.T. Cai, Ceram. Int. 44, 20877

- (2018); <https://doi.org/10.1016/j.ceramint.2018.08.093>
- [4] A. Almohammadi, A. Ashour, E.R. Shaaban, J. Ovonic. Res. 16, 21 (2020).
- [5] B.W. Duan, J.J. Shi, D.M. Li, Y.H. Luo, H.J. Wu, Q.B. Meng, Sci. China Mater. 63, 2371 (2020); <https://doi.org/10.1007/s40843-020-1385-0>
- [6] J.Z. Zhou, X. Xu, B.W. Duan, H.J. Wu, J.J. Shi, Y.H. Luo, D.M. Li, Q.B. Meng, Nano Energy 89, 106405 (2021); <https://doi.org/10.1016/j.nanoen.2021.106405>
- [7] Y. Zhao, X.X. Han, B. Xu, W. Li, J. Li, J.J. Li, M. Wang, C. Dong, P. Ju, J.S. Li, IEEE J. Photovolt. 7, 874 (2017); <https://doi.org/10.1109/JPHOTOV.2017.2675993>
- [8] J.X. Xu, J.H. Lin, C.N. Zhuang, Sol. Energy 164, 231 (2018); <https://doi.org/10.1016/j.solener.2018.02.066>
- [9] M.J. Romero, H. Du, G. Teeter, Y.F. Yan, M.M. Al-Jassim, Phys. Rev. B 84, 165324 (2011); <https://doi.org/10.1103/PhysRevB.84.165324>
- [10] M. Dimitrievska, A. Fairbrother, E. Saucedo, A. Perez-Rodriguez, V. Izquierdo-Roca, Appl. Phys. Lett. 106, 073903 (2015); <https://doi.org/10.1063/1.4913262>
- [11] A. Nagoya, R. Asahi, R. Wahl, G. Kresse, Phys. Rev. B 81, 113202 (2010); <https://doi.org/10.1103/PhysRevB.81.113202>
- [12] J.S. Park, S. Kim, Z.J. Xie, A. Walsh, Nat. Rev. Mater. 3, 194 (2018); <https://doi.org/10.1038/s41578-018-0026-7>
- [13] G. Gurieva, D.M. Tobbens, S. Levchenko, T. Unold, S. Schorr, J. Alloys Compd. 846, 156304 (2020); <https://doi.org/10.1016/j.jallcom.2020.156304>
- [14] S. Oueslati, M. Kauk-Kuusik, C. Neubauer, V. Mikli, D. Meissner, G. Brammertz, B. Vermang, J. Krustok, M. Grossberg, Sol. Energy 198, 586 (2020); <https://doi.org/10.1016/j.solener.2020.02.002>
- [15] Y.F. Tay, S.S. Hadke, M.Y. Zhang, N. Lim, S.Y. Chiam, L.H. Wong, J. Mater. Chem. A 8, 8862 (2020); <https://doi.org/10.1039/D0TA02042G>
- [16] N. Saini, J.K. Larsen, K.V. Sopiha, J. Keller, N. Ross, C. Platzer-Bjorkman, Phys. Status Solidi A 216, 1900492 (2019); <https://doi.org/10.1002/pssa.201900492>
- [17] A. Ruiz-Perona, Y. Sanchez, M. Guc, L. Calvo-Barrio, T. Jawhari, J.M. Merino, M. Leon, R. Caballero, Sol. Energy 199, 864 (2020); <https://doi.org/10.1016/j.solener.2020.02.082>
- [18] S. Yang, S.R. Wang, H. Liao, X. Xu, Z. Tang, X.Y. Li, T.B. Wang, X. Li, D. Liu, J. Mater. Sci.: Mater. Electron. 30, 11171 (2019); <https://doi.org/10.1007/s10854-019-01463-1>
- [19] K.S. Gour, O.P. Singh, J.S. Tawale, V.N. Singh, Superlattices Microstruct. 120, 54 (2018); <https://doi.org/10.1016/j.spmi.2018.05.012>
- [20] M.S. Kumar, S.P. Madhusudan, S.K. Batabyal, Sol. Energy Mater. Sol. Cells 185, 287 (2018); <https://doi.org/10.1016/j.solmat.2018.05.003>
- [21] Z.H. Su, G.X. Liang, P. Fan, J.T. Luo, Z.H. Zheng, Z.G. Xie, W. Wang, S. Chen, J.G. Hu, Y.D. Wei, C. Yan, J.L. Huang, X.J. Hao, F.Y. Liu, Adv. Mater. 32, 2000121 (2020); <https://doi.org/10.1002/adma.202000121>
- [22] C. Huang, Y. Chan, F.Y. Liu, D. Tang, J. Yang, Y.Q. Lai, J. Li, Y.X. Liu, J. Mater. Chem. A 1, 5402 (2013); <https://doi.org/10.1039/c3ta00191a>
- [23] S.H. Hadke, S. Levchenko, S. Lie, C.J. Hages, J.A. Marquez, T. Unold, L.H. Wong, Adv. Energy Mater. 8, 1802540 (2018); <https://doi.org/10.1002/aenm.201802540>

- [24] L. Qiu, J.X. Xu, X. Tian, *Nanomaterials* 9, 1520 (2019); <https://doi.org/10.3390/nano9111520>
- [25] X. Tian, J.X. Xu, *Mater. Sci. Semicond. Process.* 129, 105787 (2021); <https://doi.org/10.1016/j.mssp.2021.105787>
- [26] J.J. Fu, D.X. Kou, W.H. Zhou, Z.J. Zhou, S.J. Yuan, Y.F. Qi, S.X. Wu, *Ag, J. Mater. Chem. A* 8, 22292 (2020); <https://doi.org/10.1039/D0TA06318E>
- [27] J.Y. Tong, S.T. Wang, G. Wang, Y. Liu, Y.X. Wang, L.P. Chen, L.L. Wang, D.C. Pan, X.T. Zhang, Y.C. Liu, *Sol. Energy* 220, 882 (2021); <https://doi.org/10.1016/j.solener.2021.03.035>
- [28] X.Y. Zhao, X.H. Chang, D.X. Kou, W.H. Zhou, Z.J. Zhou, Q.W. Tian, S.J. Yuan, Y.F. Qi, S.X. Wu, *J. Energy Chem.* 50, 9 (2020); <https://doi.org/10.1016/j.jechem.2020.03.007>
- [29] G.M. Ford, Q.J. Guo, R. Agrawal, H.W. Hillhouse, *Chem. Mater.* 23, 2626 (2011); <https://doi.org/10.1021/cm2002836>
- [30] S. Kim, K.M. Kim, H. Tampo, H. Shibata, K. Matsubara, S. Niki, *Sol. Energy Mater. Sol. Cells* 144, 488 (2016); <https://doi.org/10.1016/j.solmat.2015.09.039>
- [31] K.G. Deepa, P.C. Ramamurthy, M.K. Singha, *Opt. Mater.* 98, 109492 (2019); <https://doi.org/10.1016/j.optmat.2019.109492>
- [32] D.B. Mitzi, O. Gunawan, T.K. Todorov, K. Wang, S. Guha, *Sol. Energy Mater. Sol. Cells* 95, 1421 (2011); <https://doi.org/10.1016/j.solmat.2010.11.028>
- [33] Q. Guo, G.M. Ford, W.C. Yang, B.C. Walker, E.A. Stach, H.W. Hillhouse, R. Agrawal, *J. Am. Chem. Soc.* 132, 17384 (2010); <https://doi.org/10.1021/ja108427b>
- [34] X.G. Lv, C.J. Zhu, H.M. Hao, R.J. Liu, Y.M. Wang, J.Z. Wang, *Ceram. Int.* 46, 25638 (2020); <https://doi.org/10.1016/j.ceramint.2020.07.039>
- [35] D. Mora-Herrera, M. Pal, F. Paraguay-Delgado, *Mater. Chem. Phys.* 257, 123764 (2021); <https://doi.org/10.1016/j.matchemphys.2020.123764>
- [36] G.L. Chen, W.H. Wang, S.Y. Chen, Z.Z. Whang, Z.G. Huang, B.Y. Zhang, X.K. Kong, *J. Alloys Compd.* 718, 236 (2017); <https://doi.org/10.1016/j.jallcom.2017.05.150>